WATER RESOURCES RESEARCH, VOL. 37, NO. 12, PAGES 3057–3069, DECEMBER 2001

Accurate calculation of specific discharge in heterogeneous porous media

Quanlin Zhou[1]
Faculty of Civil Engineering, Technion-Israel Institute of Technology, Haifa, Israel

Jacob Bensabat
Environmental and Water Resources Engineering, Inc., Haifa, Israel

Jacob Bear
Faculty of Civil Engineering, Technion-Israel Institute of Technology, Haifa, Israel

Abstract. Existing continuous schemes for computing the specific discharge in heterogeneous porous media result in inaccuracy in simulating the local specific discharge field at and in the vicinity of an interface between subdomains of different material properties. The domain decomposition method used in multilayered systems and a consistent scheme in a randomly heterogeneous domain are applicable only to some particular cases, such as when the material interfaces are parallel to an axis. Along a material interface, the law of refraction of streamlines, related to both the tangential and the normal specific discharge components, should be satisfied. By incorporating these interface conditions into the weak formulation of Darcy's law, two consistent numerical schemes have been developed. These schemes can be applied to accurately and efficiently simulate the specific discharge field in a heterogeneous domain with different values of the ratio of hydraulic conductivities between adjacent elements. In particular, they provide an easy way for treating aquifers with semipervious layers as a single system. Numerical simulations have been used to demonstrate the capability and accuracy of the proposed schemes. Comparison between the specific discharge fields computed by the proposed schemes and by other techniques shows that the new schemes are superior to the traditional ones.

1. Introduction

An accurate and efficient computation of a groundwater specific discharge field (q field) is crucial for the numerical simulation of contaminant transport problems. The specific discharge dominates the advective transport and is a key factor in determining the coefficients of mechanical dispersion. Most natural groundwater systems are heterogeneous. Often such a system is approximated as being composed of a number of homogeneous subdomains of different hydraulic and transport properties. At any point within each subdomain the specific discharge is continuous in all directions. However, at an interface between two different subdomains (with different material properties), only the component of the specific discharge (q component) that is normal to such an interface is continuous, while the component tangent to the interface exhibits a discontinuity as the interface is approached from both sides, obeying the refraction law of streamlines [*Bear*, 1972, 1979].

Traditionally, in finite element methods (FEMs) a q field is directly derived by numerical differentiation from the computed pressure or head distribution. The latter is linearly or bilinearly approximated. This results in a loss of 1 order of accuracy in the specific discharge computations. Furthermore, it gives rise to nonphysical discontinuities in the q components at element boundaries, even if the domain is homogeneous.

So far, most efforts have focused on the continuity of the normal flux at element boundaries. Several continuous methods have been developed. A mixed FEM formulation, applied to groundwater flow simulations by *Meissner* [1973] and *Segol et al*. [1975], requires that both heads and specific discharge constitute degrees of freedom. In a case of steady state flow the derived coefficient matrix is not positive definite. *Yeh* [1981] developed a separate FEM model for Darcy's law for the purpose of computing specific discharge, after determining the linear/bilinear head distributions by the same FEM. *Chavent and Roberts* [1991] presented a mixed-hybrid FEM model in terms of elemental average pressure/head, with edge/face pressure/head, and edge/face average flux as the dependent variables. *Cordes and Kinzelbach* [1992] developed a postprocessing patch formulation for the q field. In all these continuous schemes the continuity of the normal flux at element boundaries in a homogeneous domain can be satisfied. However, when applied to a heterogeneous domain, they may result in large errors in the local q field in the vicinity of material interfaces, since they cannot simultaneously satisfy the law of refraction of streamlines. Satisfying this law is a prerequisite for any accurate evaluation of such a local q field. Furthermore, owing to the mass balance constraint, the resulting errors in the specific discharge at material interfaces propagate to some degree to nearby regions and nodes and give rise to

[1]Now at Earth Sciences Division, Lawrence Berkeley National Laboratory, University of California, Berkeley, California, USA.

Copyright 2001 by the American Geophysical Union.

Paper number 1998WR900105.
0043-1397/01/1998WR900105$09.00

wiggling oscillations in the local q field. Sometimes this leads to a nonphysical flow field that contradicts Darcy's law as far as flow direction is concerned.

Only a small number of models consider the q field in the vicinity of material interfaces. The domain decomposition method is usually applied to simulate the flow and transport in a multilayered aquifer, visualized as being composed of a number of homogeneous subdomains. Along the internal material interfaces, boundary conditions are explicitly set and iteratively satisfied under certain specified assumptions, for example, that the specific discharge is assumed to be vertical in horizontal semipervious layers. A consistent specific discharge scheme was formulated by *Srivastava and Brusseau* [1995]. In their scheme the q component normal to a material element boundary is treated by a continuous scheme, while that tangential to such a boundary is computed by a discontinuous scheme. However, this scheme preserves the interface conditions only when the element boundaries are material interfaces which are parallel to a coordinate axis. Otherwise, the required condition of continuity of the normal flux component is not satisfied. When applied to a case with multiple material interfaces, of arbitrary shapes and with arbitrary values of the hydraulic conductivity ratio, these methods are neither efficient nor accurate.

In this paper we present two consistent specific discharge schemes. In scheme 1 the jumps in q components at any point on a material interface are analytically derived from the condition of continuity of the normal flux component at the interface and from the refraction law with respect to the tangential one. By assembling jumps at each material node (that is, a node on an interface between two materials), element by element, a global jump vector is formed and incorporated directly into the right-hand-side load (flux) vector. Meanwhile, the mesh used for head computations, and the global coefficient matrix, identical to that in the commonly used continuous FEM scheme, remain unchanged. In scheme 2 these interface conditions are taken into account in the weak formulation of specific discharge computations, using Darcy's law. Their contributions both to the global coefficient matrix and to the load vector are assembled segment by segment. In this scheme the mesh used for head computation should be modified by adding additional nodes at each material node to take into account the discontinuities in specific discharge. The proposed schemes are presented and their implementation is discussed in detail. The methods are then compared with existing ones for two-dimensional (2-D) aquifers exhibiting material discontinuities.

2. Theory

2.1. Law of Refraction of Streamlines

At an interface between two different materials in a heterogeneous anisotropic domain the normal flux and the piezometric head must satisfy the following conditions:

$$\mathbf{q}^+ \cdot \mathbf{n} = \mathbf{q}^- \cdot \mathbf{n} \tag{1}$$

$$h^+ = h^-, \tag{2}$$

where $\mathbf{q}$ is the specific discharge (expressed by Darcy's law), $\mathbf{n}$ is the unit vector normal to the interface, h is the piezometric head, and the plus and minus superscripts denote values on both sides of the interface.

From (2) it follows that

$$\mathbf{J}^+ \cdot \mathbf{s} = \mathbf{J}^- \cdot \mathbf{s}, \tag{3}$$

where $\mathbf{J}$ is the hydraulic gradient vector, and $\mathbf{s}$ is the unit vector tangential to the interface. Since the hydraulic conductivity is a tensor, $\mathbf{K}^+$ and $\mathbf{K}^-$ are invertible. The hydraulic gradient vectors, $\mathbf{J}^+$ and $\mathbf{J}^-$, may be rewritten in terms of $\mathbf{q}^+$ and $\mathbf{q}^-$:

$$\begin{aligned} \mathbf{J}^+ &= [\mathbf{K}^+]^{-1} \cdot \mathbf{q}^+ \\ \mathbf{J}^- &= [\mathbf{K}^-]^{-1} \cdot \mathbf{q}^-. \end{aligned} \tag{4}$$

By incorporating (4) into (3), we obtain the general refraction law, written for the tangential flux component in an anisotropic domain:

$$[\mathbf{K}^+]^{-1} \cdot \mathbf{q}^+ \cdot \mathbf{s} = [\mathbf{K}^-]^{-1} \cdot \mathbf{q}^- \cdot \mathbf{s} \tag{5}$$

or

$$\begin{aligned} \mathbf{q}^+ \cdot \mathbf{s} &= [\mathbf{K}^+] \cdot [\mathbf{K}^-]^{-1} \cdot \mathbf{q}^- \cdot \mathbf{s} = [\mathbf{K}'] \cdot \mathbf{q}^- \cdot \mathbf{s} = [\mathbf{K}']^T \cdot \mathbf{s} \cdot \mathbf{q}^- \\ &= [\mathbf{K}'] \cdot \mathbf{s} \cdot \mathbf{q}^-, \end{aligned} \tag{6}$$

where

$$\mathbf{K} = \begin{bmatrix} K_{xx} & K_{xy} & K_{xz} \\ K_{yx} & K_{yy} & K_{yz} \\ K_{zx} & K_{zy} & K_{zz} \end{bmatrix} \qquad \mathbf{q} = \begin{Bmatrix} q_x \\ q_y \\ q_z \end{Bmatrix} \qquad \mathbf{J} = \begin{Bmatrix} J_x \\ J_y \\ J_z \end{Bmatrix}$$

$$= \begin{Bmatrix} -\partial h/\partial x \\ -\partial h/\partial y \\ -\partial h/\partial z \end{Bmatrix} \qquad \mathbf{n} = \begin{Bmatrix} n_x \\ n_y \\ n_z \end{Bmatrix} \qquad \mathbf{s} = \begin{Bmatrix} s_x \\ s_y \\ s_z \end{Bmatrix}$$

and the superscript T denotes the transpose of vector.

In three dimensions we have two refraction laws, along two different tangential directions, $\mathbf{s}_1$, $\mathbf{s}_2$:

$$\begin{aligned} [\mathbf{K}^+]^{-1} \cdot \mathbf{q}^+ \cdot \mathbf{s}_1 &= [\mathbf{K}^-]^{-1} \cdot \mathbf{q}^- \cdot \mathbf{s}_1 \\ [\mathbf{K}^+]^{-1} \cdot \mathbf{q}^+ \cdot \mathbf{s}_2 &= [\mathbf{K}^-]^{-1} \cdot \mathbf{q}^- \cdot \mathbf{s}_2 \end{aligned} \tag{7}$$

or

$$\begin{aligned} \mathbf{q}^+ \cdot \mathbf{s}_1 &= [\mathbf{K}'] \cdot \mathbf{s}_1 \cdot \mathbf{q}^- \\ \mathbf{q}^+ \cdot \mathbf{s}_2 &= [\mathbf{K}'] \cdot \mathbf{s}_2 \cdot \mathbf{q}^-, \end{aligned} \tag{8}$$

where

$$\mathbf{s}_1 = \left\{ -\frac{n_z}{\sqrt{n_x^2 + n_z^2}}, \quad 0, \quad \frac{n_x}{\sqrt{n_x^2 + n_z^2}} \right\}^T$$

$$\mathbf{s}_2 = \left\{ 0, \quad -\frac{n_z}{\sqrt{n_y^2 + n_z^2}}, \quad \frac{n_y}{\sqrt{n_y^2 + n_z^2}} \right\}^T.$$

The complete law of refraction of streamlines, with respect to both the normal and the tangential flux, (1) and (7), can be rewritten in the form

$$\begin{aligned} &\mathbf{q}^- \cdot \mathbf{n} = \mathbf{q}^+ \cdot \mathbf{n} \\ &\mathbf{q}^- \cdot \mathbf{s}_1 = \mathbf{q}^+ \cdot \mathbf{s}_1 - (1 - [\mathbf{K}'']) \cdot \mathbf{q}^+ \cdot \mathbf{s}_1 \\ &\mathbf{q}^- \cdot \mathbf{s}_2 = \mathbf{q}^+ \cdot \mathbf{s}_2 - (1 - [\mathbf{K}'']) \cdot \mathbf{q}^+ \cdot \mathbf{s}_2, \end{aligned} \tag{9}$$

where $[\mathbf{K}''] = [\mathbf{K}^-] \cdot [\mathbf{K}^+]^{-1}$. Thus it may be rewritten in the form of jump equations:

$$\mathbf{q}_{\text{jump}} = \{[q_i]_{\text{jump}}\} = \begin{Bmatrix} q_x^+ - q_x^- \\ q_y^+ - q_y^- \\ q_z^+ - q_z^- \end{Bmatrix}$$

$$= \begin{bmatrix} \mathbf{n}^T \\ \mathbf{s}_1^T \\ \mathbf{s}_2^T \end{bmatrix} \cdot \begin{Bmatrix} 0 \\ (1 - [\mathbf{K}'']) \cdot \mathbf{q}^+ \cdot \mathbf{s}_1 \\ (1 - [\mathbf{K}'']) \cdot \mathbf{q}^+ \cdot \mathbf{s}_2 \end{Bmatrix}. \tag{10}$$

In a homogeneous domain, (10) degenerates to the condition of continuity of the q components, without the jump coupling terms:

$$[q_i]_{\text{jump}} = q_i^+ - q_i^- = 0 \qquad i = x, y, z. \tag{11}$$

For a well-posed specific discharge solution, both the continuity of the normal flux and the refraction law (or laws, in three dimensions) of the tangential fluxes have to be satisfied, although the continuity of pressure or piezometric head along a material interface is also used in head computation. For example, in the domain decomposition method applied to a multilayered aquifer, the continuity of the normal flux (iteratively satisfied) and the assumption of vertical flux in a horizontal semipervious layer are used. However, in the existing continuous specific discharge schemes, only the continuity of normal fluxes is ensured.

The specific discharge field can be calculated by Darcy's law:

$$\mathbf{q} = -\mathbf{K} \cdot \nabla h, \tag{12a}$$

subject to

$$\begin{aligned} &\mathbf{q}^+ \cdot \mathbf{n} = \mathbf{q}^- \cdot \mathbf{n} \\ &[\mathbf{K}^+]^{-1} \cdot \mathbf{q}^+ \cdot \mathbf{s} = [\mathbf{K}^-]^{-1} \cdot \mathbf{q}^- \cdot \mathbf{s} \end{aligned} \tag{12b}$$

on any material interface.

2.2. Weak Formulation of Darcy's Law

By applying the standard Galerkin FEM to Darcy's law (12a), we obtain its weak formulation:

$$\int_\Omega N_I q_i \, d\Omega = -\int_\Omega N_I K_{ij} \frac{\partial h}{\partial x_j} \, d\Omega, \tag{13a}$$

with the approximation of

$$q_i \approx \hat{q}_i = \sum_{J=1}^{L} N_J q_{iJ}, \quad h \approx \hat{h} = \sum_{J=1}^{M} N_J h_J, \tag{13b}$$

where $i = x, y$ in two dimensions; $i = x, y, z$ in three dimensions; K_{ij} is the tensor of hydraulic conductivity; N_I, N_J denote the linear basis functions; q_{iJ} is the Jth nodal specific discharge of the ith component; h_J is the Jth computed nodal head value; and L and M are the total numbers of nodes, respectively, for the computation of the specific discharge and head fields. Equation (13) may also be expressed in matrix form:

$$[A_{IJ}] \cdot \{q_{iJ}\} = \{F_{iI}\}, \tag{14a}$$

with

$$A_{IJ} = \sum_e A_{IJ}^{(e)} = \sum_e \int_{\Omega^{(e)}} N_I N_J \, d\Omega \tag{14b}$$

$$F_{iI} = \sum_e F_{iI}^{(e)} = -\sum_e \int_{\Omega^{(e)}} N_I K_{ij}^{(e)} \frac{\partial N_J}{\partial x_j} \, d\Omega \cdot \{h_J\}, \tag{14c}$$

where $[A_{IJ}]$ is the global coefficient matrix; $\{q_{iJ}\}$ is the nodal unknown vector of the ith component of $\mathbf{q}$; $\{F_{iI}\}$ is the right-hand-side load (flux) vector; $\Omega^{(e)}$ is the domain of element e; $\{h_J\}$ is the computed nodal head vector; I, J denote the global node numbering; and the superscript e denotes the element e.

The weak formulation of Darcy's law, (13), may be employed in both continuous and discontinuous FEMs, depending on the mesh used. When applied to a continuous mesh ($L = M$), such as the mesh for head computation shown in Figure 1a, it results in a continuous specific discharge scheme [*Yeh*, 1981], which gives rise to a continuous q field at any point in any direction. When applied to a discontinuous mesh ($L > M$), such as the mesh shown in Figures 1b and 2a, it becomes a discontinuous FEM and leads to a discontinuous specific discharge scheme. In the proposed consistent schemes the interface conditions, (12b), are incorporated into this weak formulation of Darcy's law.

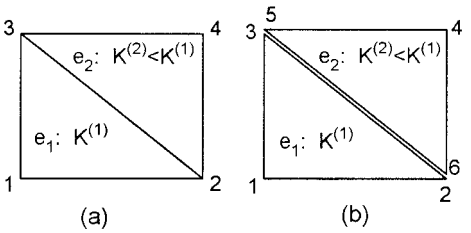

Figure 1. Scheme 1: (a) a continuous mesh and (b) a discontinuous mesh.

3. Implementation in a 2-D Locally Isotropic Porous Media

In what follows, the proposed approaches will be demonstrated in the case of a 2-D flow in a locally isotropic aquifer. Extension to 3-D flow requires more algebra but is straightforward.

In two dimensions the refraction law, (6), may be written in terms of the unit tangential vector: $\mathbf{s} = \{n_y, -n_x\}^T$. When applied to an isotropic domain, both the continuity of the normal flux component, (1), and the refraction law for the tangential one, (6), may be expressed, respectively, in the form:

$$q_n - q_n^- = 0 \qquad q_s - \frac{K}{K^-} q_s^- = 0 \tag{15}$$

or

$$n_x q_x + n_y q_y = n_x q_x^- + n_y q_y^-; \quad n_y q_x - n_x q_y = \frac{K}{K^-}(n_y q_x^- - n_x q_y^-). \tag{16}$$

In the jump form the law of refraction may be written as

$$\begin{aligned} \begin{Bmatrix} [q_x]_{\text{jump}} \\ [q_y]_{\text{jump}} \end{Bmatrix} &= \begin{bmatrix} n_x & n_y \\ n_y & -n_x \end{bmatrix} \cdot \begin{Bmatrix} 0 \\ \left(1 - \dfrac{K^-}{K}\right)(q_x n_y - q_y n_x) \end{Bmatrix} \\ &= \left(1 - \frac{K^-}{K}\right) \begin{Bmatrix} n_y^2 q_x - n_x n_y q_y \\ n_x^2 q_y - n_x n_y q_x \end{Bmatrix}, \end{aligned} \tag{17}$$

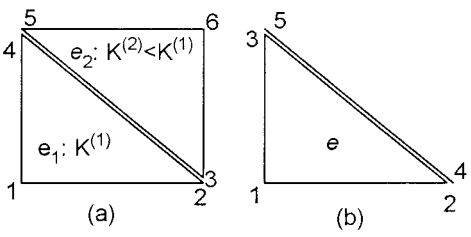

Figure 2. Scheme 2: (a) a discontinuous mesh and (b) a local nodal numbering for an element e with a material interface.

where q_n, q_s are the normal and tangential components of the specific discharge $\mathbf{q}$; q_x, q_y are the components of $\mathbf{q}$ in the x, y directions; and K is the hydraulic conductivity. Here, the values of q components and K without a superscript are for the side of higher hydraulic conductivity.

For the presentation of both schemes, let us consider a domain with two triangular elements separated by a material interface. The meshes for schemes 1 and 2 are shown in Figures 1 and 2.

3.1. Scheme 1

At any point on a material interface, we rewrite the law of refraction of streamlines, (17), in the general form of jump equations:

$$[q_i]_{\text{jump}} = q_i - q_i^- = \left(1 - \frac{K^-}{K}\right)(n_j^2 q_i - n_i n_j q_j) \qquad (18)$$

$$i = x, y \qquad j = y, x,$$

where q_i^- are the specific discharge components on the low conductivity side of the interface, and q_i are those on the higher conductivity side. Here no summation is used; $[q_i]_{\text{jump}}$ result from the discontinuities in the specific discharge on both sides.

In a discontinuous mesh (Figure 1b) an element with at least one material node is defined as a material element. We shall refer to the element with the high hydraulic conductivity as the basic element, while that with the lower conductivity will be referred to as the dependent element. Furthermore, the specific discharge at a material node of a basic element will be regarded as a primary variable, while the specific discharge at the same location but on the other side will be regarded as a dependent variable. Thus all dependent variables can be determined by their corresponding primary nodal variables and nodal jumps. For example, in Figure 1b the q components at dependent node 5 can be expressed by those at its corresponding primary node 3:

$$q_{x5} = q_{x3} - [q_{x3}]_{\text{jump}} = q_{x3} - \left(1 - \frac{K^{(2)}}{K^{(1)}}\right)(n_y^2 q_{x3} - n_x n_y q_{y3}) \qquad (19)$$

$$q_{y5} = q_{y3} - [q_{y3}]_{\text{jump}} = q_{y3} - \left(1 - \frac{K^{(2)}}{K^{(1)}}\right)(n_x^2 q_{y3} - n_x n_y q_{x3}), \qquad (20)$$

where $K^{(1)}$, $K^{(2)}$ are the hydraulic conductivities of elements 1 and 2, respectively. By such nodal jumps all the unknown dependent variables at additional material nodes in a discontinuous mesh may be expressed by their corresponding primary ones.

To demonstrate this scheme, let us consider as an example the dependent material element 2 in Figure 1b. Its elemental matrix system equations, by the discontinuous FEM procedure, obtained from the weak formulation of Darcy's law, (13), are

$$[A_{I'J'}^{(2)}] \cdot \begin{Bmatrix} q_{i4} \\ q_{i5} \\ q_{i6} \end{Bmatrix} = \{F_{iI'}^{(2)}\}, \qquad (21)$$

where $[A_{I'J'}^{(2)}]$ and $\{F_{iI'}^{(2)}\}$ are the elemental coefficient matrix and load vector, determined by (14); I', J' (I', $J' = 1$–3) are the local node numbers; and q_{iJ} ($J = 4, 5, 6$) are the global node values. Taking into account the jumps in q components at the material node pairs (2, 6) and (3, 5), such matrix system in (21) is converted into the same form as in a general continuous FEM, in the form

$$[A_{I'J'}^{(2)}] \cdot \begin{Bmatrix} q_{i4} \\ q_{i3} \\ q_{i2} \end{Bmatrix} = \{F_{iI'}^{(2)}\} + \{G_{iI'}^{(2)}\}, \qquad (22)$$

where $\{G_{iI'}^{(2)}\}$ is the elemental jump vector, defined by

$$\{G_{iI'}^{(2)}\} = \begin{Bmatrix} G_{i1}^{(2)} \\ G_{i2}^{(2)} \\ G_{i3}^{(2)} \end{Bmatrix} = \left(1 - \frac{K^{(2)}}{K^{(1)}}\right)[A_{I'J'}^{(2)}] \begin{Bmatrix} 0 \\ n_j^2 q_{i3} - n_i n_j q_{j3} \\ n_j^2 q_{i2} - n_i n_j q_{j2} \end{Bmatrix}.$$

With the introduction of such elemental jump vectors, the coefficient matrix, the unknown and load vectors of a dependent element, are converted into the same form as those obtained by a general continuous FEM formulation of Darcy's law. It is apparent that the contribution to the elemental jump vector of a dependent element is only from material nodes. For all basic and nonmaterial elements the elemental jump vector is zero, and their elemental system equations are the same as those derived by a continuous FEM procedure.

By assembling we obtain the global coefficient matrix and the total load vector:

$$[A_{IJ}]\{q_{iJ}^*\} = \{F_{iI}\} + \{G_{iI}\}, \qquad (23)$$

where $\{q_{iJ}^*\}$ is the unknown vector, and $\{G_{iI}\}$ is the global jump vector. The latter results from the discontinuities in q components between the dependent and primary nodal values at all material nodes. It is obtained by assembling the contributions from all the dependent elements having an interface (interfaces) or a single material node. In the former case the normal vector of such an interface is used. In the latter, however, an averaged normal vector, obtained from all interfaces connecting at such a node, is used. All nonzero elements in $\{G_{iI}\}$ correspond to material nodes and their connected nodes in dependent material elements. It should be noted that here the unknown vector, $\{q_{iJ}^*\}$, which is different from $\{q_{iJ}\}$ in (14), consists of the unknowns at all nonmaterial nodes, and the primary unknowns, rather than averaged values appearing in a continuous scheme, at material ones. Without the jump vector, $\{G_{iI}\}$, in a homogeneous domain, (23) is identical to (14) of the continuous scheme, and the $\{q_{iJ}^*\}$'s are the nodal averaged values. Thus the continuous scheme can be taken as a special case of our scheme 1, with the identical values on both sides of element edges.

The mesh depicted in Figure 1b, constructed by adding some additional nodes at the original material nodes in the continuous mesh in Figure 1a, is used to demonstrate the methodology for taking into account specific discharge discontinuities. However, it is not necessary to construct such an additional mesh and node numbering for the specific discharge computations. In fact, the mesh used for head computation is also valid for these computations. In (23) the number of degrees of freedom of any q component is the same as the node number in the mesh shown in Figure 1a. After solving (23) the dependent nodal values at additional nodes (e.g., nodes 5 and 6) at material interfaces, on the side of the dependent elements, may be explicitly derived by using (18).

In general, there is a coupling between the equations that evaluate $\{q_{xJ}\}$ and $\{q_{yJ}\}$ by the interface conditions in a heterogeneous domain, and their solutions are coupled by the jump vector, $\{G_{iI}\}$, consisting of some elements in both $\{q_{xJ}\}$

and $\{q_{yJ}\}$. An iterative solution technique is then used as follows:

1. Assemble the global coefficient matrix $[A_{IJ}]$ and the load vector $\{F_{iI}\}$ $(i = x, y)$ and solve (14) independently for initial solutions $\{q_{xJ}^{(l)}\}$ and $\{q_{yJ}^{(l)}\}$ $(l = 0)$.
2. Set $l = l + 1$.
3. Assemble the global jump vector $\{G_{xI}^{(l)}(\{q_{xJ}^{(l-1)}\}, \{q_{yJ}^{(l-1)}\})\}$ material element by element, solve (23), and update the solution $\{q_{xJ}^{(l)}\}$.
4. Assemble the global jump vector $\{G_{yI}^{(l)}(\{q_{xJ}^{(l)}\}, \{q_{yJ}^{(l-1)}\})\}$ material element by element, solve (23), and update the solution $\{q_{yJ}^{(l)}\}$.
5. Check the convergence of iterations for $\{q_{xJ}^{(l)}\}$ and $\{q_{yJ}^{(l)}\}$; if it is convergent, stop; otherwise, go to (2) and repeat (2)–(5).

This coupling disappears when all material interfaces are parallel to a coordinate axis. For the q component along such an axis, the jump vector, $\{G_{iI}\}$, consisting only of such a component, does not disappear because a discontinuity between the primary and the dependent q components also exists. However, for the vertical component, the jump vector $\{G_{iI}\}$ is zero, since the normal flux component is continuous. Therefore, in a multilayered system with such particular horizontal interfaces, the improvement in accuracy in the simulations of local q fields, in the vicinity of material interfaces, does not reduce the solution efficiency.

3.2. Scheme 2

In this scheme the weak formulation of the specific discharge computation is obtained by incorporating the interface conditions, (15), into the weak formulation, (13), for a discontinuous mesh (Figure 2a), in the form

$$\int_\Omega N_I q_i \, d\Omega + \lambda_n \int_\Gamma N_I (q_n - q_n^-) \, d\Gamma + \lambda_s \int_\Gamma N_I \left(q_s - \frac{K}{K^-} q_s^- \right) d\Gamma = -\int_\Omega N_I K \frac{\partial h}{\partial x_i} \, d\Omega, \tag{24}$$

where Γ is the set of material interfaces, and λ_n, λ_s are penalty weights (>0). When a coordinate axis is parallel to a material interface, $\lambda_n = 0$ for the computation of the q component along such axis, while $\lambda_s = 0$ for the other component. Otherwise, generally, $\lambda_n = \lambda_s = \lambda$.

The interface conditions, (16), may be rewritten in the forms

$$n_I q_i - n_I q_i^- = -n_J q_j + n_J q_j^- \tag{25a}$$

$$n_J q_i - \frac{K}{K^-} n_J q_i^- = n_I q_j - \frac{K}{K^-} n_I q_j^-. \tag{25b}$$

To keep the problem well-posed, it is necessary to ensure that the diagonals of the elemental and the global matrices are positive. Thus, by combining (25a) and (25b), we obtain

$$\alpha_1 q_i + \alpha_2 q_i^- = \alpha_3 q_j + \alpha_4 q_j^-, \tag{26}$$

where

$$\alpha_1 = |n_i| + |n_j|, \qquad \alpha_2 = -\left(|n_i| + \frac{K}{K^-} |n_j| \right),$$

$$\alpha_3 = -n_j \operatorname{sign}(n_i) + n_i \operatorname{sign}(n_j),$$

and

$$\alpha_4 = n_j \operatorname{sign}(n_i) - \frac{K}{K^-} n_i \operatorname{sign}(n_j).$$

To include the interface contributions for the element on the side of a material interface with the lower hydraulic conductivity, we apply (26). However, in order to keep the final system matrix positive definite, for the element on the side with higher hydraulic conductivity, we have to change (26) to

$$-\alpha_2 q_i - \alpha_1 q_i^- = -\alpha_4 q_j - \alpha_3 q_j^-. \tag{27}$$

With these modifications of interface conditions, the weak formulation, (24), is rewritten as

$$\int_\Omega N_I q_i \, d\Omega + \lambda\alpha_1 \int_\Gamma N_I q_i \, d\Gamma + \lambda\alpha_2 \int_\Gamma N_I q_i^- \, d\Gamma = -\int_\Omega N_I K \frac{\partial h}{\partial x_i} \, d\Omega + \lambda\alpha_3 \int_\Gamma N_I q_j \, d\Gamma + \lambda\alpha_4 \int_\Gamma N_I q_j^- \, d\Gamma. \tag{28}$$

For the purposes of demonstration, let us consider element e in Figure 2b. The interface terms may be expressed as

$$\alpha_1^e [B_{I'J'}^e] \cdot \begin{Bmatrix} q_{i2}^e \\ q_{i3}^e \end{Bmatrix} + \alpha_2^e [B_{I'J'}^e] \cdot \begin{Bmatrix} q_{i4}^e \\ q_{i5}^e \end{Bmatrix} = \alpha_3^e [B_{I'J'}^e] \cdot \begin{Bmatrix} q_{j2}^e \\ q_{j3}^e \end{Bmatrix} + \alpha_4^e [B_{I'J'}^e] \cdot \begin{Bmatrix} q_{j4}^e \\ q_{j5}^e \end{Bmatrix}, \tag{29}$$

where

$$B_{I'J'}^e = \int_{\Gamma^e} N_{I'} N_{J'} \, d\Gamma = \begin{bmatrix} b_{11}^e & b_{12}^e \\ b_{21}^e & b_{22}^e \end{bmatrix} \qquad I', J' = 2, 3,$$

in which $q_{iJ'}^e$ denotes the nodal values of the ith q component at the local node J' $(J' = 2\text{–}5)$, and Γ^e is the material edge of the material element e. By combining the contributions from the interior of the element and along the material interface, we obtain the elemental matrix system:

$$[A_{I'J'}^e] \cdot \begin{Bmatrix} q_{i1}^e \\ q_{i2}^e \\ q_{i3}^e \end{Bmatrix} + \lambda \begin{bmatrix} \alpha_1^e b_{11}^e & \alpha_1^e b_{12}^e & \alpha_2^e b_{11}^e & \alpha_2^e b_{12}^e \\ \alpha_1^e b_{21}^e & \alpha_1^e b_{22}^e & \alpha_2^e b_{21}^e & \alpha_2^e b_{22}^e \end{bmatrix} \cdot \begin{Bmatrix} q_{i2}^e \\ q_{i3}^e \\ q_{i4}^e \\ q_{i5}^e \end{Bmatrix} = \{F_{iI'}^e\} + \lambda \begin{bmatrix} 0 & 0 \\ b_{11}^e & b_{12}^e \\ b_{21}^e & b_{22}^e \end{bmatrix} \cdot \begin{Bmatrix} \alpha_3^e \alpha_{j2}^e + \alpha_4^e q_{j4}^e \\ \alpha_3^e q_{j3}^e + \alpha_4^e q_{j5}^e \end{Bmatrix}. \tag{30}$$

Therefore, in this scheme, both the original coefficient matrix and the load vector of an interface-connecting material element are modified in order to satisfy interface conditions. After assembling contributions to the global coefficient matrix and to the right-hand-side load vector from interior elements, we assemble contributions of each material interface from the material elements on both sides of such an interface. Finally, we obtain the global matrix system:

$$[A_{IJ} + A_{IJ\Gamma}] \cdot \{q_{iJ}^{**}\} = \{F_{iI} + F_{iI\Gamma}\}, \tag{31}$$

where $[A_{IJ\Gamma}]$, $\{F_{iI\Gamma}\}$ are the portions of the global coefficient matrix and the right-hand-side load vector contributed by all

material interfaces, respectively, and $\{q_{iJ}^{**}\}$ is the unknown vector. This unknown vector consists of the averaged specific discharge variables at all nonmaterial nodes, and the variables at material nodes and their corresponding additional nodes.

Selecting an appropriate value for the weight λ is essential in order to ensure the two interface conditions, while not degenerating the nature of the problem, since such conditions are only weakly incorporated into the weak formulation of Darcy's law. It should be large enough so as to satisfy these conditions. On the other hand, if the selected value is too large, the effect of Darcy's law is overridden, and a large round-off error may result. Practically, there is a wide optimal range for λ values, such that it is easy to select an appropriate one.

As in scheme 1, the solutions for the q components in the x and y directions, $\{q_{xJ}\}$ and $\{q_{yJ}\}$, are generally coupled because of the interface conditions. An iteration algorithm is used as follows:

1. Assemble the global coefficient matrix $[A_{IJ}]$ and the load vector $\{F_{iI}\}$ $(i = x, y)$ element by element in the discontinuous mesh and then assemble $[A_{IJ\Gamma}]$ interface segment by segment and solve (14) independently for initial solutions $\{q_{xJ}^{(l)}\}$ and $\{q_{yJ}^{(l)}\}$ $(l = 0)$.
2. Set $l = l + 1$.
3. Assemble the load vector $\{F_{xI\Gamma}^{(l)}(\{q_{yJ}^{(l-1)}\})\}$, interface segment by segment, solve (31), and update the solution $\{q_{xJ}^{(l)}\}$.
4. Assemble the load vector $\{F_{yI\Gamma}^{(l)}(\{q_{xJ}^{(l)}\})\}$, solve (31), and update the solution $\{q_{yJ}^{(l)}\}$.
5. Check the convergence of iterations for $\{q_{xJ}^{(l)}\}$ and $\{q_{yJ}^{(l)}\}$; if it is convergent, stop; otherwise go to (2) and repeat (2)–(5).

Only when all material interfaces are parallel to a coordinate axis are their solutions uncoupled. As seen in Figure 2a we need to add additional nodes at the same location of each material node in the continuous mesh used for head computation. Furthermore, we have to satisfy the condition that the total node number at that location be identical to the number of materials connecting to such a node. Meanwhile, we reconstruct a new node numbering in such a way that the numbering of all the nodes in the different materials at the same location be consecutive so that the increase in bandwidth of the system matrix may be the smallest.

3.3. Treatment of Singular Nodes

When applied to a heterogeneous domain with a number of nonintersecting straight material interfaces, the proposed consistent schemes perform very well. However, if any two interfaces, with different normal vectors, intersect within the study domain, we have a singular point. In such a case it is impossible to satisfy interface conditions at material element edges connecting at such a point. Theoretically, at such singular point, two different streamlines intersect, and the specific discharge becomes infinite. Moreover, the local q field in its vicinity is very complex. Most singular points are artificially created, either by parameter regionalization and geometrical conceptualization, while developing the conceptual model, or in the process of mesh generation and averaging of element parameters in the numerical model. To demonstrate different methods for treating singular points, we consider three cases:

Case 1 is a singular point resulting from parameter regionalization and geometrical conceptualization. In this case the hydraulic conductivity varies continuously around such a point, and no real singular point exists. A sharp material interface is assumed only for simplification. In such a case the specific discharge at the "singular point" is not infinite, and the local flow around it is continuous. Thus it is not necessary to incorporate interface conditions on the material edges of its connecting elements. Furthermore, if necessary, we may take into account the continuous variations in the hydraulic conductivity within the elements connected by the singular point, rather than assuming a sharp variation in hydraulic conductivity along the material interface.

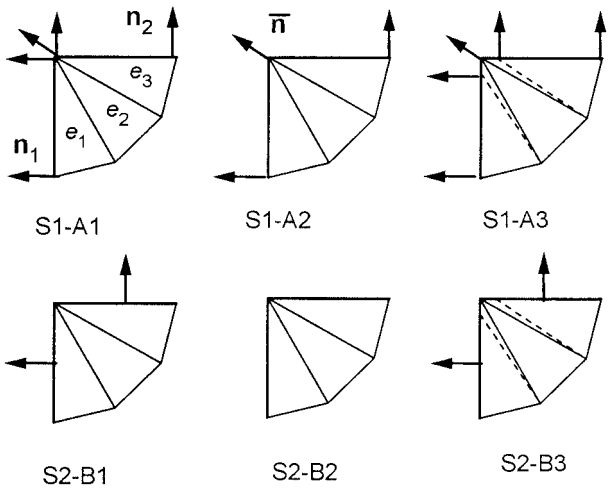

Figure 3. Alternatives for treating singular points in schemes 1 and 2.

Case 2 is a singular point resulting from mesh generation and element parameter averaging. Most curved material interfaces smoothed by parameter regionalization are represented by straight lines in a numerical model. Around such a singular point, mesh refinement may be used to smooth the variations in the normal vectors at material elements edges.

Case 3 is a real singular point. Such a point seldom exists in a porous medium. Whenever it does occur, it produces only slight variations in the normal vector. Thus such a singular point cannot cause a difficulty in treating the local q field. On the other hand, close to a singular point with a large variation in the normal vector, Darcy's law is not valid, as the specific discharge becomes very large. Thus capturing the singularity in the numerical model is not essential.

Let us discuss alternatives for treating singular points in both schemes (Figure 3). In scheme 1 (S1) there are two possibilities (alternatives 1 and 2) for setting the normal vector at a singular point: (1) In A1 for a dependent element with such an interface connecting with such a point (e.g., e_1 and e_3), the normal vector of this interface ($\mathbf{n}_1$ or $\mathbf{n}_2$) is used. For a dependent element with only such a singular node, an average normal

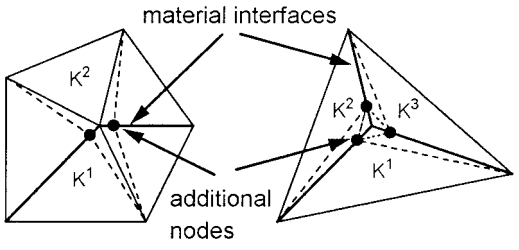

Figure 4. Local mesh refinement around a singular node.

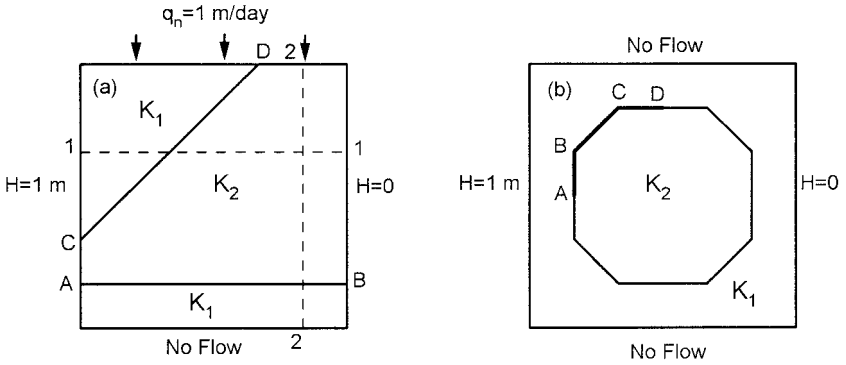

Figure 5. Boundary conditions and material compositions in (a) example 1 and (b) example 2.

vector (e.g., e_2), $\bar{\mathbf{n}}$, obtained from all its connecting interfaces, is used. (2) In A2, only the average normal vector is used for such a singular point, independent of the element to which such a point belongs.

In scheme 2 (S2), which is based on how interface conditions are considered at the material edges of elements connecting with a singular point, we also have two alternatives (alternatives 3 and 4): (1) In B1, interface conditions are incorporated into the weak formulation, (24) or (28), for all material edges of elements. However, at the edges connecting with such a singular point, these conditions can never be met. On the contrary, because of the specific discharge averaging at this point, the error propagation along the material interface will be worsened, causing the conditions not to be met also at several adjacent material edges. (2) In B2, the interface conditions at the material edges connecting with the singular point are relaxed. Then, the conditions are not satisfied only at such edges, and the propagating error is freed to the extent that it is controlled by Darcy's law.

Because of the large specific discharge variations around a singular point, an averaged specific discharge at such point cannot control a sharp variation (discontinuity) in specific discharge or its peaks when the point is approached from its connecting material edges, especially for a coarse mesh. To capture such peaks, as well as the complex local q field around such a point, we use a simple technique for mesh refinement around a singular point. We add a node on each interface in the vicinity of the singular point, and create additional elements so the triangulation remains conforming (Figure 4). In the following numerical experiments, such mesh refinement techniques (S1-A3, S2-B3) and the alternatives S1-A2 and S2-B2 are presented and compared.

4. Numerical Experiments

The accuracy of the proposed consistent schemes is demonstrated by comparing specific discharge fields in heterogeneous domains computed by four different schemes. All the schemes are based on the head distribution calculated by a standard Galerkin FEM with triangular elements and linear basis functions.

In a continuous scheme (CS) [*Yeh*, 1981] a separate application of Galerkin FEM to Darcy's law is utilized. The mesh, node numbering, and basis functions for head computation are used. A set of M linear equations (M is the number of nodes) is obtained and solved for each q component: $\{q_{xJ}\}$ and $\{q_{yJ}\}$. The resulting components are linear within each element and continuous at all element boundaries.

In a discontinuous scheme (DS) the mesh and node numbering used in head computation are modified by adding nodes

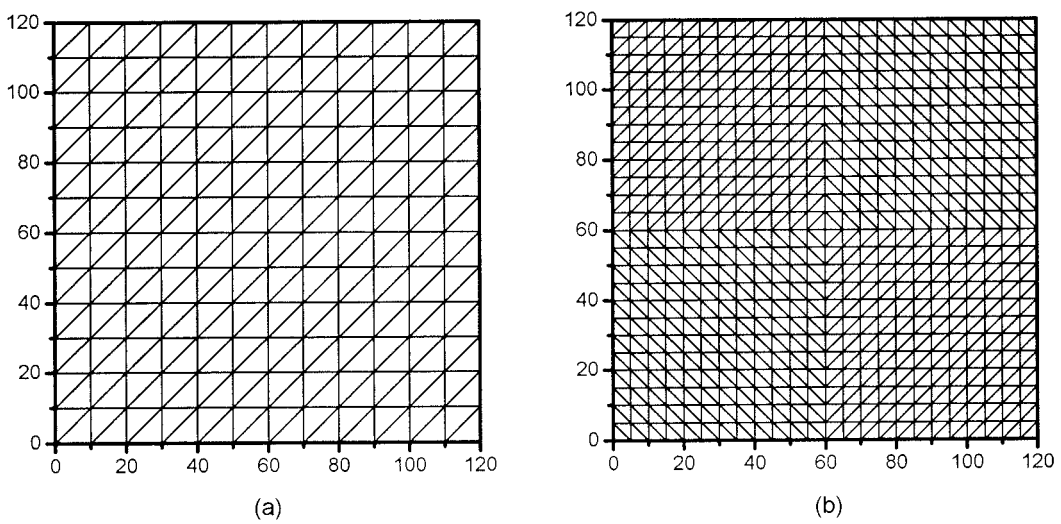

Figure 6. The meshes used to compute the piezometric head and the specific discharge fields (default) in (a) example 1 and (b) example 2.

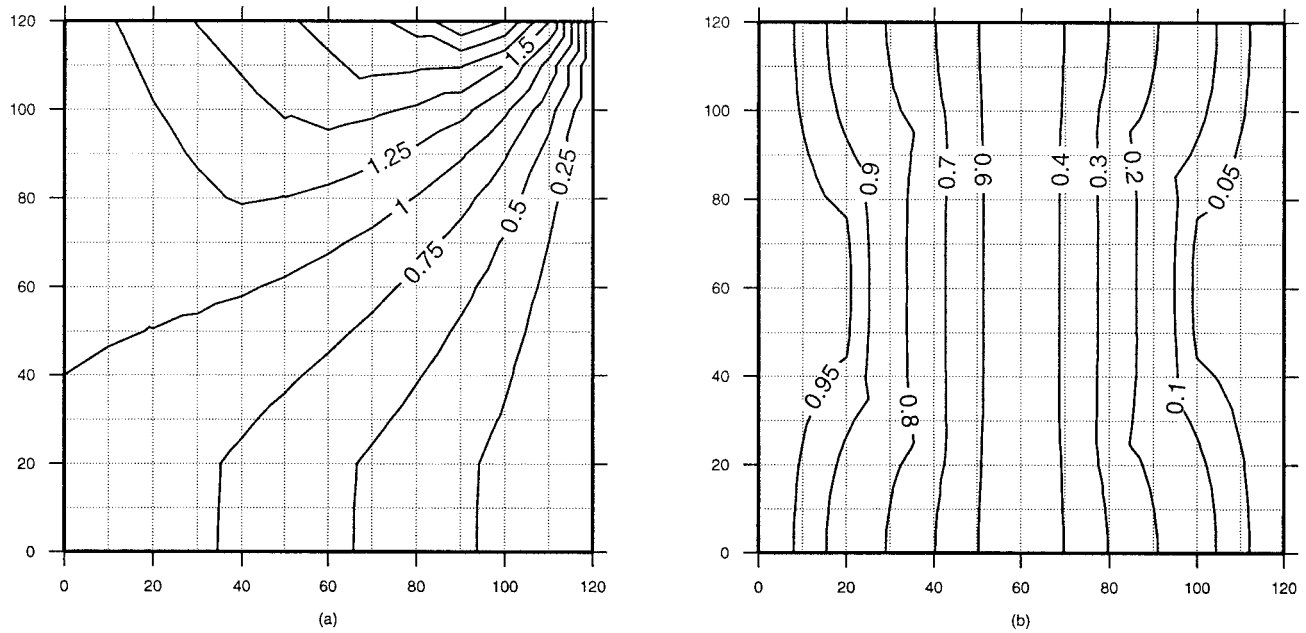

Figure 7. Contour maps of the piezometric head in (a) Example 1, and (b) Example 2.

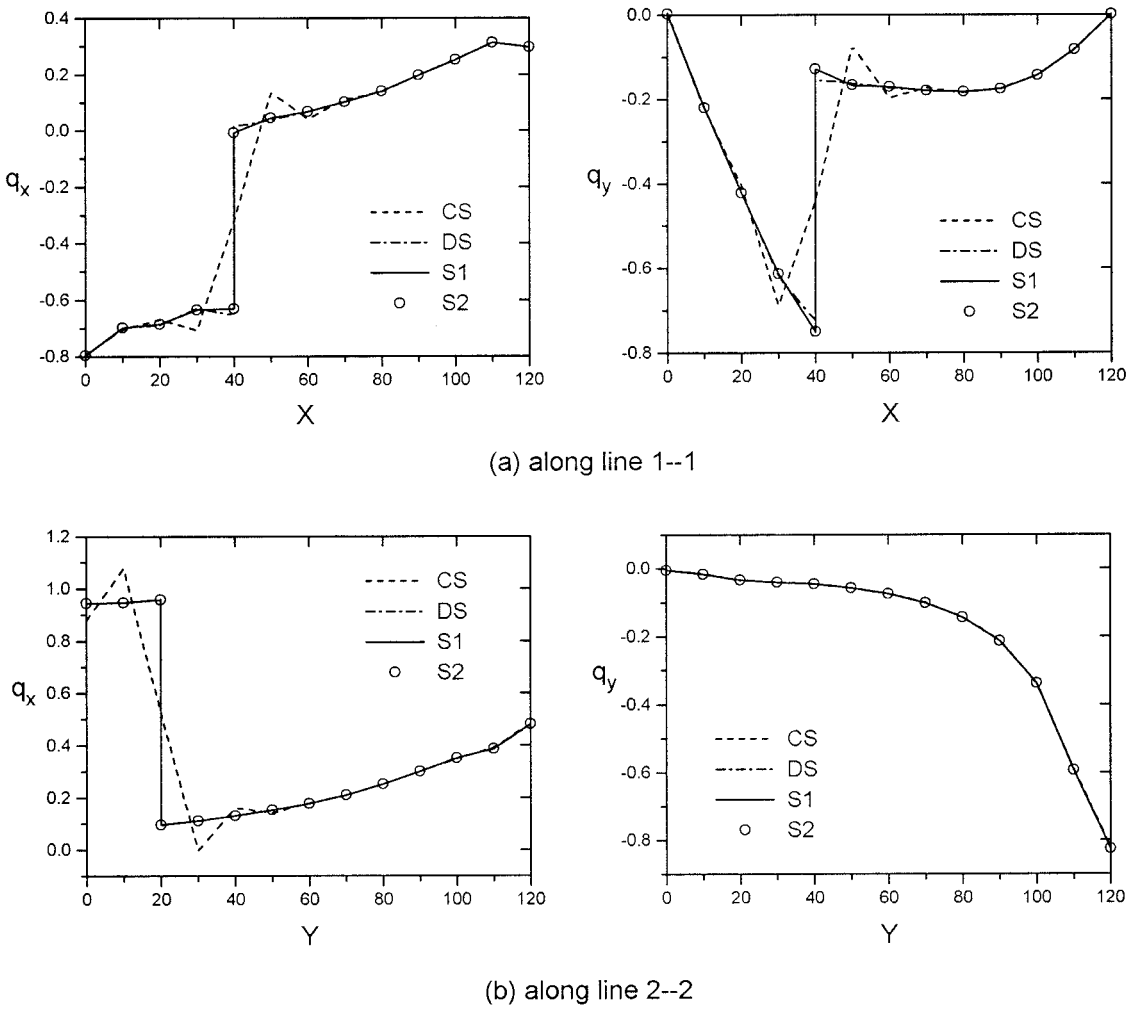

Figure 8. Variations of the specific discharge components along (a) line 1–1 and (b) line 2–2.

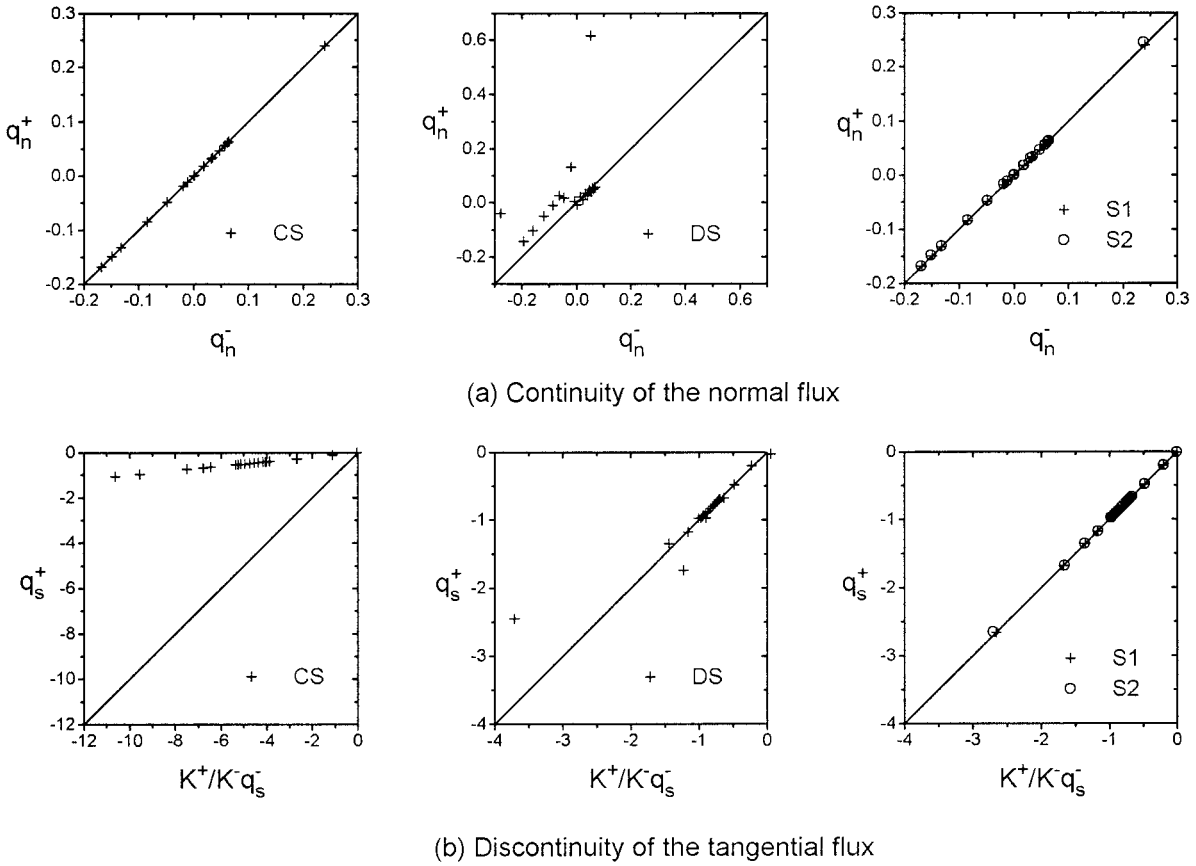

Figure 9. Conditions of the law of refraction of streamlines at all material nodes in the different methods: (a) continuity of the normal flux and (b) discontinuity of the tangential flux component.

at each material node in order to take into account discontinuity in specific discharge on both sides of a material interface. A set of $L = M + M_m$ linear equations is derived and solved (M_m is the number of additional nodes at all material nodes). Along a material interface in a heterogeneous domain, each q component is generally discontinuous.

In the above two methods, each q component is solved independently, and no iteration between different components is needed.

In scheme 1 (S1) we use the same mesh as in CS. After an iterative solution between all q components, we obtain the averaged specific discharge at each nonmaterial node, and the primary specific discharge at each material node on the basic element side. Then we explicitly derive the dependent one at such a material node on the other side by nodal jumps.

In scheme 2 (S2) we use the same mesh as in DS. An iteration is also generally needed in the solutions for all q components. For each component a set of $M + M_m$ linear equations has to be solved.

Two experiments are considered for the comparison. In all the examples an isotropic aquifer, having the shape of a square with the dimensions of 120 m by 120 m, is considered (Figure 5). It has a fixed head ($H = 1.0$ m) at the left boundary, a lower fixed head ($H = 0$ m) at the right boundary, and no flow across the bottom boundary. It has a specified inflow flux ($q_n = 1.0$ m/d) in example 1 (see below) and no flow in example 2 across the top boundary. Different material compositions within it are used to demonstrate the capacity of the proposed schemes to simulate a heterogeneous domain with complex material compositions and interfaces of arbitrary shapes. The piezometric head distribution is obtained by applying the standard Galerkin finite element method, with linear basis functions, to the steady flow

$$\nabla \cdot (K \cdot \nabla h) = 0. \tag{32}$$

In example 1 a mesh with 288 ($12 \times 12 \times 2$) uniform vertical triangular elements of $10m \times 10m$ is used. In example 2 a finer mesh, with 1152 elements of $5m \times 5m$, is employed (Figure 6). The piezometric head fields in Figure 7, calculated for these meshes, are the basis for the derivation of and discussion on the specific discharge fields of the four methods. Unless otherwise specified, these default meshes are also used in deriving the specific discharge fields.

4.1. Example 1

For the first example the domain contains two kinds of materials, separated by a horizontal AB and a skew straight CD material interfaces (Figure 5a). Lines 1–1 and 2–2 are used to show variations in q components. The high hydraulic conductivity is $K_1 = 100.0$ m/d, and the lower is $K_2 = 10.0$ m/d.

CS and S1 result in the same or very close specific discharge fields in the homogeneous subdomains which are far from the material interfaces (not shown). However, differences are significant for the local q fields in the vicinity of these interfaces. In addition, S1 and S2 produce the same q fields in the entire domain, even at the material interfaces. DS gives a small difference at interfaces and in the nearest element wide strip along the interfaces, in comparison with S1 and S2.

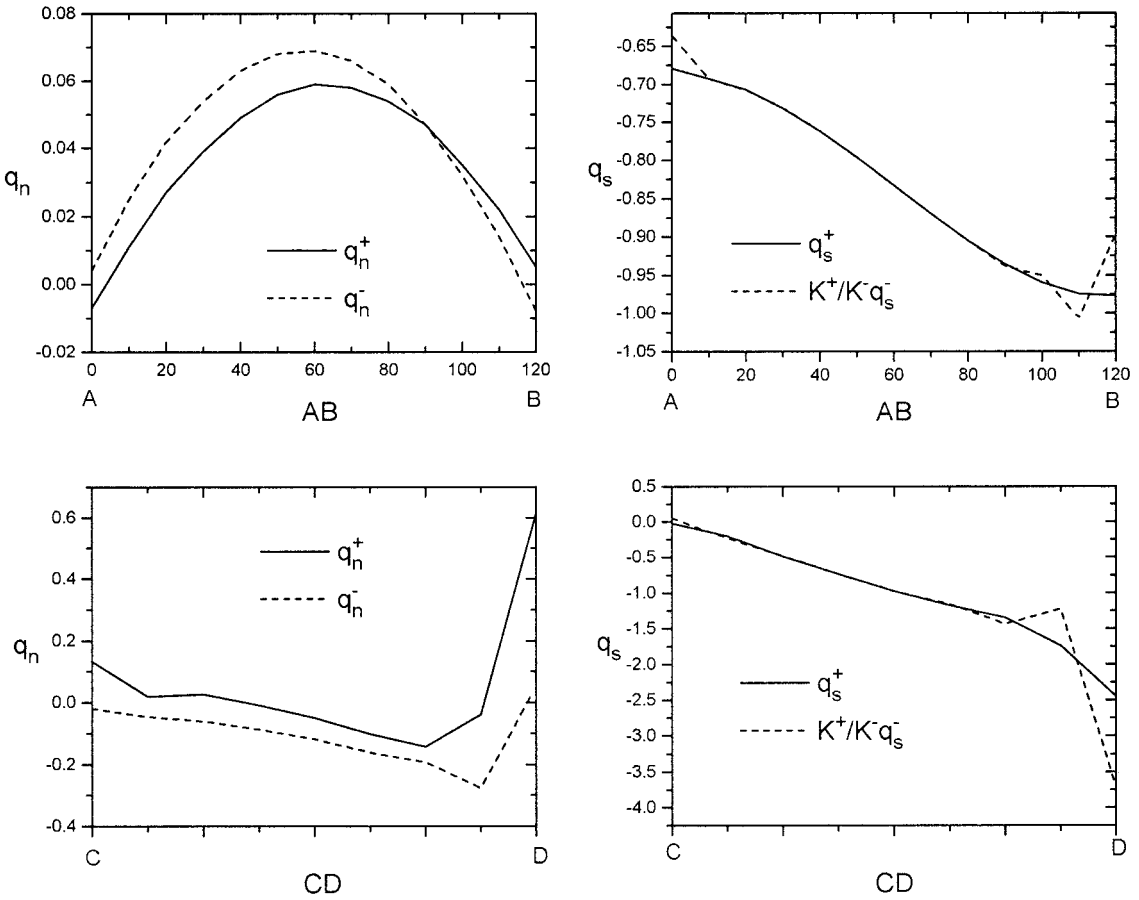

Figure 10. Variations of the normal and tangential components of specific discharge along AB and CD material interfaces by the discontinuous scheme (DS).

Figure 8 shows error propagation from material interfaces. S1 and S2 give rise to the same smooth variations of q components along lines 1–1 and 2–2, except that they exhibit physically consistent discontinuities at material interfaces. Within an influenced strip of the nearest 6–8 elements along the interfaces, CS results in large errors and oscillatory wiggling specific discharge variations. The reason is that for the same head load determined by the computed head distribution, CS, by averaging, increases the specific discharge at a material node on the side of low hydraulic conductivity. Thus it reduces the specific discharge at the adjacent nodes connecting with such a material node, and increases that at the nodes behind such adjacent nodes. On the other hand, CS reduces the material nodal specific discharge on the side of higher hydraulic conductivity and results in additional error waves, whose amplitudes are gradually attenuated with the distance from such a material node. Besides the difference at material interfaces, the largest difference between CS and S1 occurs at the nearest nodes connecting with material ones. Moreover, on the side of lower hydraulic conductivity, the absolute amplitude of error waves is slightly larger, and the influence of material interfaces is also larger, since the specific discharge is relatively smaller than that on the other side. Figure 8b shows that CS results in the same q component, q_y, as S1 when the interface is vertical to such a particular direction. Outside such a strip, CS produces a q field that is very close to that of S1. In DS small differences occur at material interfaces and in their adjacent elements, in comparison with the differences in S1. Thus the propagation of errors in simulating the specific discharge at interfaces is much smaller and closer-reaching than in CS.

Figure 9 shows that on both material interfaces, S1 and S2 preserve the law of refraction of streamlines, namely, the continuity of the normal flux components and the discontinuity of the tangential ones. CS preserves the continuity of the normal components. However, it does not meet the required condition of the discontinuity of the tangential ones, since its derived q components in any direction are continuous at any point. Figures 9 and 10 show that DS does not satisfy the continuity of the normal fluxes. Along material interfaces the outflow from the side of high hydraulic conductivity is greater than the influx to the side of lower hydraulic conductivity. Thus the discontinuous scheme is not mass conserving. On the other hand, it preserves the law of refraction of streamlines with respect to the tangential components, except at nodes close to boundaries. In the particular case of the horizontal interface (AB), DS can satisfy the law of refraction of streamlines for the x component; this conclusion is the same as that obtained by *Srivastava and Brusseau* [1995].

Figure 11 shows the effects of a material interface on the computed x component along 1–1 for different values of the ratio of hydraulic conductivities K_1/K_2 with $K_1 = 100$ m/d and $K_2 = 1$, 50, 100, and 1000 m/d. In the case of $K_1 = K_2 = 100$ m/d, CS, S1, and S2 provide the same variations of the q component, q_x, and no discontinuity in this component at the material interface ($x = 40$ m) occurs. DS gives rise to a nonphysical discontinuity at the CD interface because in a

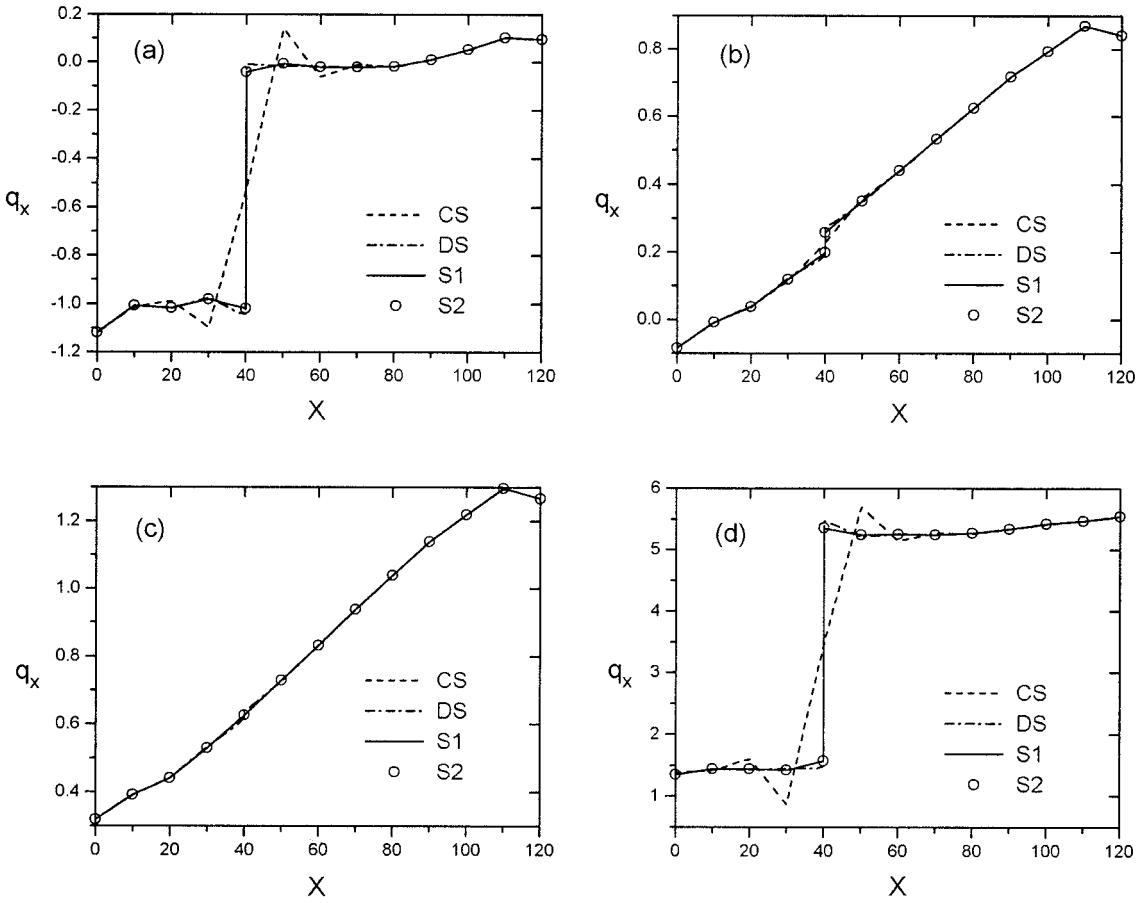

Figure 11. Effect of material interfaces on the x component of specific discharge along line 1–1 for different hydraulic conductivity ratio K_1/K_2 (K_1 = 100 m/d): (a) K_2 = 1, (b) K_2 = 50, (c) K_2 = 100, and (d) K_2 = 1000 m/d.

general case, the discontinuous scheme cannot preserve the required continuity of the normal flux. A similarly influenced strip with a width of about six to eight elements exists in CS as long as there exists a discontinuity in hydraulic conductivity (Figures 11a, 11b, and 11d). However, when K_2 is close to K_1 (K_2 = 50), the jumps in q components become smaller. Thus the difference in specific discharge solutions between CS and S1 also becomes smaller and the influenced strip is narrower.

In Figure 12 the range and degree of the effect of the CD material interface on the computed x component of the specific discharge along 1–1 are shown for CS and S1 for meshes with 72, 288, 1152, 4608, and 18,432 uniform elements. For CS the influenced strip becomes narrower with the process of mesh refinement. For instance, in the last four finer meshes, such strips are, respectively, about 80, 40, 20, and 10 m wide in the x direction. However, within the influenced strip in the

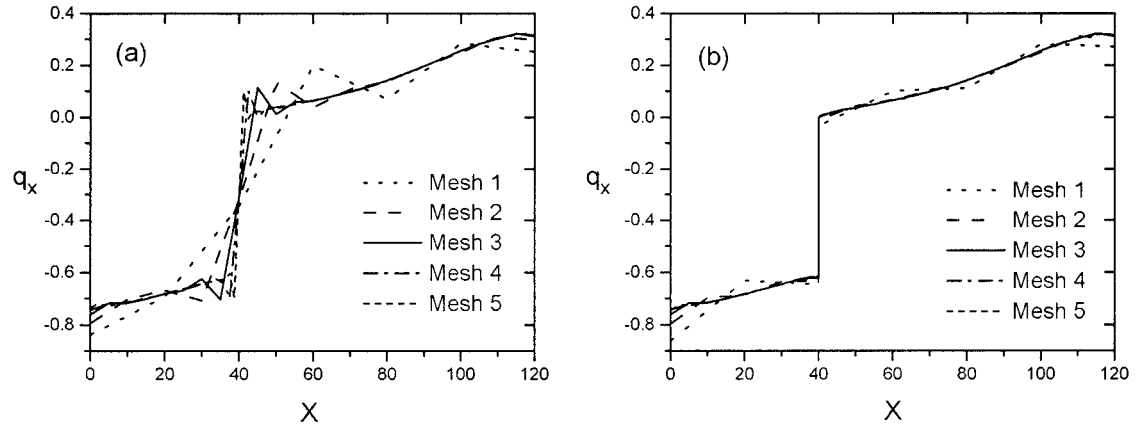

Figure 12. Effect of material interfaces on the x component of specific discharge along line 1–1 for different meshes by (a) the continuous scheme (CS) and (b) scheme 1 (S1).

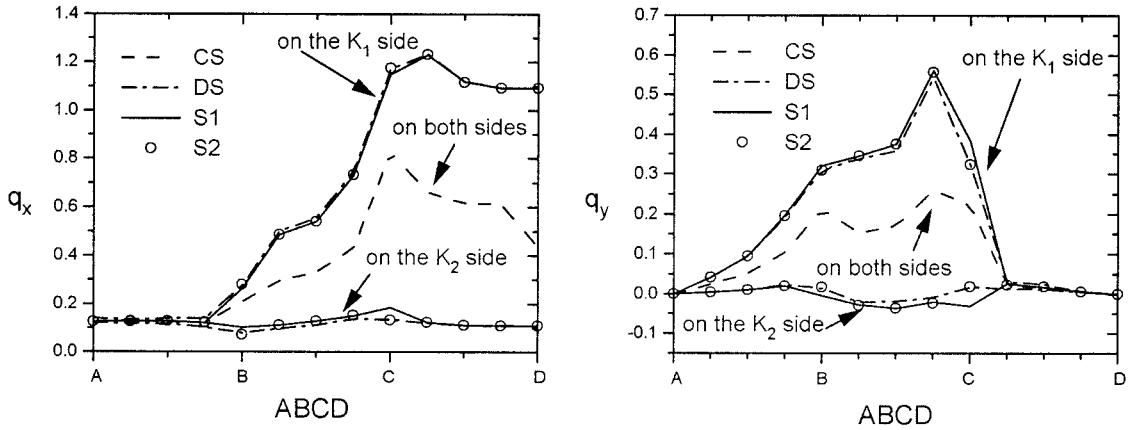

Figure 13. Variations of the specific discharge components along the segment ABCD of material interface.

finest mesh, large differences always occur among the solutions with different meshes. Especially, the amplitude of error waves decreases only slightly with the process of mesh refinement, and the errors at the nodes nearest to the interface ($x = 40$ m) cannot be reduced by mesh refinement. From this point of view CS is not efficient for deriving accurate local q fields near material interfaces. In S1 the solutions converge very fast with mesh refinement. For the last three finer meshes the same solution is obtained, except for some difference at boundary nodes. Even the solution with the second mesh is close to those of the last three ones. Thus we may obtain an accurate q field in a heterogeneous domain using a much coarser mesh by S1 than by CS. In particular, the solutions by CS, for different meshes, approach gradually those obtained by S1, with a relatively coarser mesh, for example, with 1152 elements.

Iterations among the solutions for different q components are needed in S1 and S2. Usually, S2 requires only about 4 iterations, as it is more efficient than S1, which generally needs about 10 iterations. This may be concluded from the fact that S1 explicitly considers interface conditions, while S2 converges fast by employing a larger weight, λ. The efficiency of the proposed schemes depends also on the percentage of material nodes (of the total number of nodes) and the regularity of the shapes of the material interfaces. On the other hand, the proposed consistent schemes can derive an accurate solution by a coarser mesh, compared to the much finer mesh (as seen in Figure 12) required by the commonly used continuous scheme (CS). From this aspect, the proposed schemes may be more efficient than the continuous one.

4.2. Example 2

This example involves an octagonal block of a different hydraulic conductivity embedded in an otherwise homogeneous medium (Figure 5b). There are eight singular points. By default, alternatives S1-A2 and S2-B2 are used for treating such points in S1 and S2, respectively. The segment ABCD is a material interface used for analyzing the variations in q components at material nodes around the singular points B and C in different schemes.

CS leads to large differences within a six-element-wide influenced strip along the entire material interface, in comparison with S1 (not shown). The largest errors occur at the nearest nonmaterial nodes connecting with a material node. Some negative values of the x component of specific discharge occur on the side of low hydraulic conductivity. This contradicts Darcy's law and the computed head contour as far as flow direction is concerned. In addition (not shown), we find the solutions by S1 and S2 to be very close, except for a slight difference at some singular points. This difference results from the different methods used for treating singular points, as mentioned above (S1-A2 and S2-B2). In DS a small difference at the material interface and within its nearest two-element-wide strip is caused by the fact that it separates the connection between both sides of the interface and thus cannot meet the law of refraction of streamlines.

Regarding mass balance, all schemes except DS are mass-conservative. When an error in specific discharge (actually, mass flux) occurs for some reason at a node, this error will propagate to its connecting nodes and lead to a negative error, thus resulting in a oscillatory local q field. Because of the mass balance constraint, the effect of the original error will finally disappear from an influenced strip. We may conclude that the solutions by all schemes for the specific discharge out of the influenced strip of material interface are very close to each other and may even be considered identical.

Figure 13 shows the differences in the q components along the segment ABCD of the material interface among the various schemes. CS gives the same x component of the specific discharge along AB and the same y component along CD as S1 and S2, except at the singular points and their connecting material nodes, since in these cases CS gives the physically (normal) continuous q component. At all other nodes it gives rise to large differences by averaging the specific discharge on both sides of the interface. DS results in the same y component along AB and x component along CD as S1, since it preserves the law of refraction of streamlines related to the tangential components. However, it leads to a small difference in the x component along AB and the y component along CD. At BC and all material nodes connecting with singular points, DS also gives a small difference in comparison with S1. S1 and S2 give very close results in all the segments except at the singular points B and C.

Figure 14a shows the improvement in the solutions for the x component in S1 with mesh refinement. Around the singular point B, the specific discharge varies sharply, and no large differences in the specific discharge at point B are seen among the different meshes. However, around the singular point C, a high peak of specific discharge occurs, and the specific discharge around it is more complicated. Thus it is difficult to

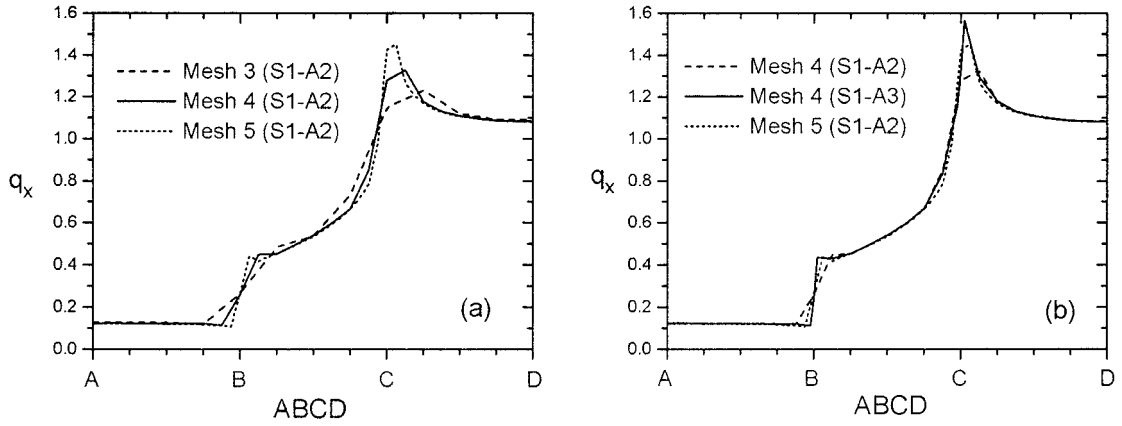

Figure 14. Comparisons of q_x along ABCD by (a) different meshes and (b) alternatives for treating singular points.

capture such a peak, and the differences among the different meshes are significant. At other material nodes, except for the singular-point-connecting ones, the specific discharge is close. Figure 14b shows the comparisons of the solution for the x component of specific discharge between the different alternatives for treating singular points, S1-A2 and S1-A3. Apparently, S1-A3 captures the peak of specific discharge around point C and the sharp variation of specific discharge around point B more efficiently than S1-A2. Therefore the local mesh refinement around singular points is an efficient alternative for treating a singular point with a high peak of specific discharge or sharp variations in specific discharge.

5. Conclusions

The existing continuous and discontinuous schemes for the calculation of specific discharge cannot simultaneously preserve the law of refraction of streamlines along a material interface in heterogeneous porous media. All of them give rise to an inaccuracy in the local specific discharge field in the vicinity of such an interface. Two consistent schemes are proposed by incorporating both interface conditions into the weak formulation of Darcy's law in two different ways. The performance of these schemes is compared with that of some often-used techniques through two flow situations. The results indicate that both consistent schemes can produce an accurate evaluation of the local specific discharge field in the vicinity of material interfaces and satisfy the interface conditions at such interfaces. In addition, they provide identical results in simulating a homogeneous subregion far from the material interface to others by existing schemes.

These proposed schemes can simulate specific discharge fields in a complex natural groundwater aquifer with any number of material compositions and interfaces of arbitrary shapes. Near a singular point, additional nodes on material interface are added and mesh refinement is used to greatly reduce its adverse effect on the accuracy of simulations. As a result, the interface conditions are met on most of a material interface. Only on a very small portion near the singular node are such conditions not satisfied. However, the mass balance around such a node is preserved.

Because of the coupling of different specific discharge components on material interfaces by the interface conditions, iterations are required for the solutions for these components. However, only a small number of iterations is usually needed. If the material nodes constitute a large percentage of the total number of nodes, the coupling iterations may take more CPU time than the noniterative schemes. On the other hand, the proposed schemes can save more CPU time in a coarser mesh in order to reach the same accuracy that is arrived at by existing schemes in a much finer mesh. They can also require less CPU time in other aspects of transport simulations to get the same final results (e.g., in the case of density coupling in seawater intrusion).

In a multilayered aquifer with any number of horizontal semipervious layers, no coupling iteration is needed among the solutions for different specific discharge components in the proposed schemes. Therefore they can be applied to accurately and efficiently simulate the specific discharge field and transport in such a system. By taking the whole system as a single domain, the proposed schemes avoid some assumptions and iterations required in the commonly used domain decomposition method.

References

Bear, J., *Dynamics of Fluids in Porous Media*, Elsevier Science, New York, 1972.

Bear, J., *Hydraulics of Groundwater*, McGraw-Hill, New York, 1979.

Chavent, G., and J. E. Roberts, A unified physical presentation of mixed, mixed-hybrid finite element and standard finite difference approximations for the determination of velocities in waterflow problems, *Adv. Water Res.*, *14*(6), 329–348, 1991.

Cordes, C., and W. Kinzelbach, Continuous groundwater velocity fields and path lines in linear, bilinear, and trilinear finite elements, *Water Resour. Res.*, *28*(11), 2903–2911, 1992.

Meissner, U., A mixed finite element model for use in potential flow problems, *Int. J. Numer. Methods Eng.*, *6*, 467–473, 1973.

Segol, G., G. E. Pinder, and W. G. Gray, A Galerkin finite element technique for calculating the transient position of the salt water front, *Water Resour. Res.*, *11*(2), 343–347, 1975.

Srivastava, R., and M. L. Brusseau, Darcy velocity computations in the finite element method for multidimensional randomly heterogeneous porous media, *Adv. Water Res.*, *18*(4), 191–201, 1995.

Yeh, G. T., On the computation of Darcian velocity and mass balance in the finite element modeling of groundwater flow, *Water Resour. Res.*, *17*, 1529–1534, 1981.

J. Bear, Faculty of Civil Engineering, Technion-Israel Institute of Technology, Haifa 32000, Israel.

J. Bensabat, EWRE, P.O. Box 6770, Haifa 31067, Israel. (jbensabat@ewre.com)

Q. Zhou, Earth Sciences Division, Lawrence Berkeley National Laboratory, University of California, Berkeley, 1 Cyclotron Road, MS 90-1116, Berkeley, CA 94577, USA. (qlzhou@lbl.gov)

(Received July 8, 1998; revised November 16, 1998;
accepted November 30, 1998.)